Science of the Total Environment 590–591 (2017) 540–553

Contents lists available at ScienceDirect

Science of the Total Environment

journal homepage: www.elsevier.com/locate/scitotenv

High resolution profile of inorganic aqueous geochemistry and key redox zones in an arsenic bearing aquifer in Cambodia

Laura A. Richards [a,*], Daniel Magnone [a], Chansopheaktra Sovann [b], Chivuth Kong [c], Sebastian Uhlemann [d,e], Oliver Kuras [d], Bart E. van Dongen [a], Christopher J. Ballentine [f], David A. Polya [a]

[a] School of Earth and Environmental Sciences and Williamson Research Centre for Molecular Environmental Science, The University of Manchester, Williamson Building, Oxford Road, Manchester M13 9PL, UK
[b] Department of Environmental Science, Royal University of Phnom Penh, Phnom Penh, Cambodia
[c] Faculty of Agricultural Economics and Rural Development, Royal University of Agriculture, Phnom Penh, Cambodia
[d] British Geological Survey, Environmental Science Centre, Keyworth, Nottingham NG12 5GG, UK
[e] ETH Zurich, Institute of Geophysics, Sonneggstrasse 5, 8092 Zurich, Switzerland
[f] Department of Earth Sciences, University of Oxford, South Parks Road, Oxford OX1 3AN, UK

HIGHLIGHTS

- Key changes in inorganic aqueous geochemistry monitored at high spatial resolution.
- Groundwater arsenic is highly heterogeneous and often exceeds health guidelines.
- Arsenic associated with iron, sulfate and dissolved oxygen along natural flowpaths.
- Geochemical models used to determine model redox equilibrium and mineral saturation.
- Key characterized aquifer redox zones can vary with depth, lithology, site & season.

GRAPHICAL ABSTRACT

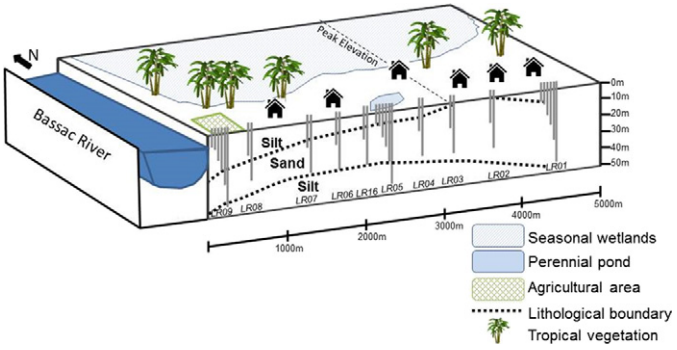

ARTICLE INFO

Article history:
Received 9 January 2017
Received in revised form 24 February 2017
Accepted 27 February 2017
Available online 9 March 2017

Editor: F.M. Tack

Keywords:
Arsenic
Redox zones
Groundwater quality
Groundwater monitoring
PHREEQC
Redox modelling

ABSTRACT

Arsenic contamination of groundwaters in South and Southeast Asia is a major threat to public health. In order to better understand the geochemical controls on the mobility of arsenic in a heavily arsenic-affected aquifer in northern Kandal Province, Cambodia, key changes in inorganic aqueous geochemistry have been monitored at high vertical and lateral resolution along dominant groundwater flow paths along two distinct transects. The two transects are characterized by differing geochemical, hydrological and lithological conditions. Arsenic concentrations in groundwater are highly heterogenous, and are broadly positively associated with iron and negatively associated with sulfate and dissolved oxygen. The observed correlations are generally consistent with arsenic mobilization by reductive-dissolution of iron (hydr)oxides. Key redox zones, as identified using groupings of the PHREEQC model equilibrium electron activity of major redox couples (notably ammonium/nitrite; ammonium/nitrate; nitrite/nitrate; dissolved oxygen/water) have been identified and vary with depth, site and season. Mineral saturation is also characterized. Seasonal changes in groundwater chemistry were observed in areas which were (i) sandy and of high permeability; (ii) in close proximity to rivers; and/or (iii) in close proximity to ponds. Such changes are attributed to monsoonal-driven surface-groundwater interactions and are

* Corresponding author.
E-mail address: laura.richards@manchester.ac.uk (L.A. Richards).

http://dx.doi.org/10.1016/j.scitotenv.2017.02.217

consistent with the separate provenance of recharge sources as identified using stable isotope mixing models.

1. Introduction

Millions of people in South and Southeast Asia are chronically exposed to dangerous concentrations of geogenic arsenic in groundwater, at levels which exceed the World Health Organization drinking water provisional guideline of 0.13 μM (10 $\mu g \cdot L^{-1}$) (Smedley and Kinniburgh, 2002; Charlet and Polya, 2006; World Health Organization, 2011; Ravenscroft et al., 2009). The arsenic in these shallow aquifers is widely thought to be released into groundwaters following the reductive dissolution of arsenic-bearing Fe(III) minerals (Islam et al., 2004), a process which is driven by metal reducing bacteria and fuelled by organic matter providing an electron donor (Charlet and Polya, 2006; Islam et al., 2004; Postma et al., 2007; Bhattacharya et al., 1997; Rowland et al., 2009). The sub-surface location where arsenic mobilization takes place (*e.g.* near surface *versus* in-aquifer), and the subsequent controls on arsenic mobility, remains vigorously debated (Harvey et al., 2002; McArthur et al., 2011; Neumann et al., 2011; Datta et al., 2011; Lawson et al., 2013), not in the least because of the spatial heterogeneity of arsenic observed in affected aquifers, but also because of questions regarding the nature of the organic matter implicated in arsenic release (Rowland et al., 2009; Harvey et al., 2002; Lawson et al., 2013; Nickson et al., 1998; McArthur et al., 2004; Neumann et al., 2009; van Dongen et al., 2008; Rowland et al., 2007; Al Lawati et al., 2013; Al Lawati et al., 2012); the high sensitivity of arsenic mobilization to redox environments (Lee et al., 2008; Mukherjee et al., 2008; Sharif et al., 2008; Ying et al., 2015; Gulens et al., 1978; Smedley and Edmunds, 2002); and the potential impact of large-scale groundwater abstraction on future arsenic hazard (Harvey et al., 2002; Polya and Charlet, 2009).

Aqueous and sediment redox environments crucially influence the mobility and spatial variability of arsenic in groundwater (Lee et al., 2008; Mukherjee et al., 2008; Sharif et al., 2008; Ying et al., 2015; Gulens et al., 1978; Smedley and Edmunds, 2002; Cherry et al., 1979; Kocar et al., 2008; Polizzotto et al., 2008; Tufano et al., 2008). In the Mekong Delta of Cambodia, anoxic sediment conditions created by extensive monsoonal flooding cause favourable anaerobic processes such as arsenate respiration (a microbial process significantly contributing to arsenic mobilization *via* reductive dissolution of arsenic-bearing iron minerals) to occur (Charlet and Polya, 2006; Islam et al., 2004; Postma et al., 2007; Bhattacharya et al., 1997; Rowland et al., 2009; Ying et al., 2015). Cyclic seasonally induced oxidation and reduction of near-surface sediments has been proposed to lead to eventual arsenic drawdown to deeper parts of the aquifer in circum-Himalayan groundwaters (Ying et al., 2015; Kocar et al., 2008; Polizzotto et al., 2008). In-aquifer geochemistry also has a significant and complex impact on the mobility of arsenic, and delineating redox boundaries can assist in understanding arsenic speciation and mobility (Lee et al., 2008). A number of common groundwater redox classifications exist (Lee et al., 2008; Bjerg et al., 1995; Christensen et al., 2000; Chen and Liu, 2003), however these classifications are often based on a single parameter or limited set of parameters, such as dissolved oxygen (DO) and/or nitrate. These may not be applicable to other locations with different groundwater characteristics, be able to encompass seasonal changes, or be sufficient to describe the complex nature of arsenic mobilization and/or speciation. Furthermore, chemometrically defined redox zones, as defined by trends in various redox-sensitive solutes such as arsenic, methane, iron, manganese, sulfate, nitrate and ammonium, can overlap as result of overprinting of different redox conditions, leading to partial equilibrium conditions and complex interactions among electron acceptors (Mukherjee et al., 2008), as well as affecting kinetic limitations on redox processes and/or metastable species (Balzer, 1982; O'Day et al., 2004; Borch et al., 2010).

Thus, detailed characterization of the groundwater geochemistry and interacting redox processes is essential to understanding the key controls on arsenic transport in these aquifers. The aim of this paper is to characterize the inorganic aqueous environment in a heavily arsenic-contaminated aquifer in northern Kandal Province, Cambodia, at a high spatial resolution along two distinct transects ("T-Sand" which is sand-dominated and "T-Clay" which is clay-dominated) in relatively close proximity which have differing geochemical and hydrological characteristics. The specific objectives are to: (i) develop high resolution profiles of groundwater geochemistry along groundwater flowpaths across the distinct transects T-Sand and T-Clay; (ii) identify areas of elevated arsenic occurrence and the corresponding relationship to other inorganic groundwater parameters (such as iron, nitrogen-containing compounds, DO and sulfate); (iii) identify and characterize key site-specific redox zones affecting groundwater geochemistry; and (iv) quantify the seasonal/monsoonal influence on these key redox zones.

2. Methods and materials

2.1. Field site description

The field sites are located along two distinct transects (Table 1), T-Sand and T-Clay, in the Kien Svay district of northern Kandal Province, Cambodia, south east of Phnom Penh, in an area generally well-known to be heavily affected by arsenic in its aquifers (Lawson et al., 2013;

Table 1
Description of field sites in northern Kandal Province, Cambodia along two distinct transects (T-Sand and T-Clay).

Transect	T-Sand	T-Clay
Number of sites	10	5
Wells installed (N)	32	17
Depth range (m)	6–45	6–30
Length of transect (m)	~4500	~2500
Wells sampled pre-monsoon (N)	24	11
Wells sampled post-monsoon (N)	26	12
Surface water proximity & description	Perpendicular to Bassac River, large pond near one site, heavily affected in parts by seasonal wetlands	Perpendicular to Mekong River, large pond near one site, heavily affected in parts by seasonal wetlands
Lithological description	Sand/silt dominated, near-surface sand windows in some locations	Clay cap (of variable thickness) over sandy aquifer
Previous characterization	Limited (Richards et al., 2015; Richards et al., 2017)	Well-characterized (Lawson et al., 2013; van Dongen et al., 2008; Polya and Charlet, 2009; Kocar et al., 2008; Polizzotto et al., 2008; Polya et al., 2003; Polya et al., 2005; Charlet and Polya, 2006; Tamura et al., 2007; Appelo and Postma, 1993; Benner et al., 2008; Rowland et al., 2008; Lawson et al., 2016)
Site names	LR01–LR09, LR16	LR10–LR14

van Dongen et al., 2008; Polya and Charlet, 2009; Kocar et al., 2008; Polizzotto et al., 2008; Polya et al., 2003; Polya et al., 2005; Charlet and Polya, 2006; Tamura et al., 2007; Appelo and Postma, 1993; Benner et al., 2008; Rowland et al., 2008; Lawson et al., 2016). Schematics of T-Sand and T-Clay (Fig. 1) show the profiles as well as the prevalent land influences along each transect (including seasonal wetlands, ponds, agricultural areas and proximity to major rivers). A site map is provided (Fig. S1). Transects were initially selected on the basis of electrical resistivity tomography (AGI SuperSting R8, USA, with dipole-dipole measurement configuration and data inversion using Res2dInv Geotomo Software (Loke and Barker, 1995)), which enabled identification of areas broadly classified by differences in lithology (defined by their resistivity characteristics) and inferred hydraulic conductivity (Fig. 2). Transects have been oriented to be broadly parallel with inferred major groundwater flowpaths on the basis of topography.

2.2. Well installation and sediment sampling and analysis

The installation of well clusters along inferred groundwater flowpaths along T-Sand and T-Clay occurred in November 2013–February 2014, using manual rotary drilling as previously described (Richards et al., 2015). All wells are named in a notation system of LRXX-YY where XX represents the site ID and YY is the depth (m) of the well. The depths of the wells ranged from 6–30 m on T-Clay and from 6–45 m on T-Sand, a depth range which was selected on the basis of the scale of key changes previously observed (Lawson et al., 2013; Polizzotto et al., 2008; Benner et al., 2008). All wells contain 1 m of screening to ensure that groundwater sampled is derived from near the depth of the well and to maintain a high resolution of groundwater monitoring and sampling (Richards et al., 2015). Wet sediment cores were collected at the time of drilling (Richards et al., 2015) and particle size analysis was conducted on dried and sieved (<2 mm) sediment subsamples at the British Geological Survey (Keyworth, UK), using laser diffraction (LS 13 320 Laser Diffraction Particle Size Analyzer, Beckman Coulter, UK) and data interpretation and statistical analysis using the Gradistat_v8 software package (Richards et al., 2017; Blott and Pye, 2001; Vandenberghe et al., 1997; Rawlins et al., 2009).

2.3. Groundwater and surface water sampling and analysis

Surface water samples and groundwater samples from flushed and developed wells (Richards et al., 2015) were collected during two sampling seasons: (i) pre-monsoon in May–June 2014; and (ii) post-monsoon in November–December 2014. Groundwater (from a depth range of 6 to 45 m) and surface waters were sampled using a submersible pump (MP1, Grundfos) for wells <9 m in depth, and a peristaltic pump (Easy Load II Peristaltic Pump, Geotech Environmental Equipment, Inc.) was used to sample shallower wells. Drilling-related contamination was shown to be minimal (typically <3%) based on a lithium chloride tracer and corrections for drilling-related contamination were not made (Richards et al., 2015). Water sampling campaigns were conducted both immediately before and after the monsoon season (as much as logistically possible) in order to improve the understanding of the geochemical implications of the seasonal monsoon shifts, which have been shown to affect the groundwater hydrology and redox conditions in near-surface sediments near the study area (Ying et al., 2015; Kocar et al., 2008; Polizzotto et al., 2008).

Measurements of pH, *Eh*, DO and electrical conductivity/temperature were collected *in-situ* using a multimeter (Professional Plus Series Portable Multimeter, YSI), equipped with compatible probes/sensors (605101, 605102, 605203 and 605301, respectively, YSI, UK) and a flow cell (603059, YSI, UK) and recorded every minute prior to and

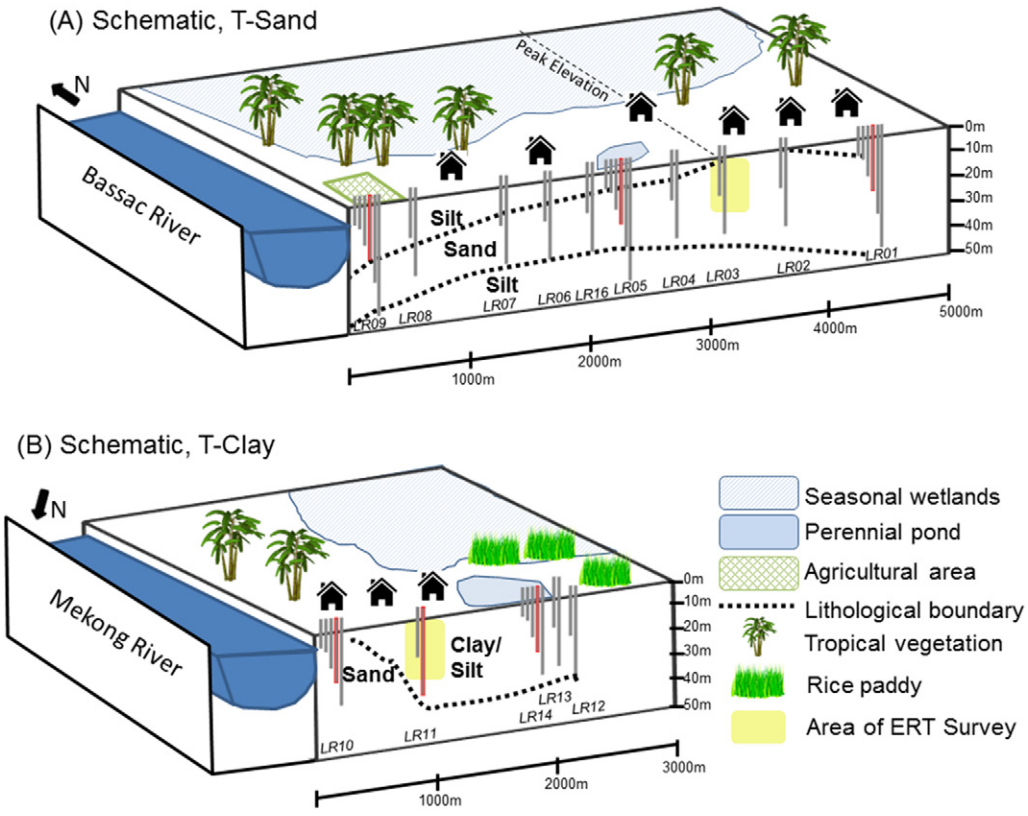

Fig. 1. Conceptual schematic of (A) T-Sand and (B) T-Clay in northern Kandal Province, Cambodia illustrating the spatial construction of well nests for groundwater monitoring and sampling. Land influences include seasonal wetlands, ponds, agricultural areas and proximity to the Bassac River. Red lines indicate locations of piezometric dataloggers and yellow squares indicate approximate selected zones of ERT surveys as shown on Fig. 2.

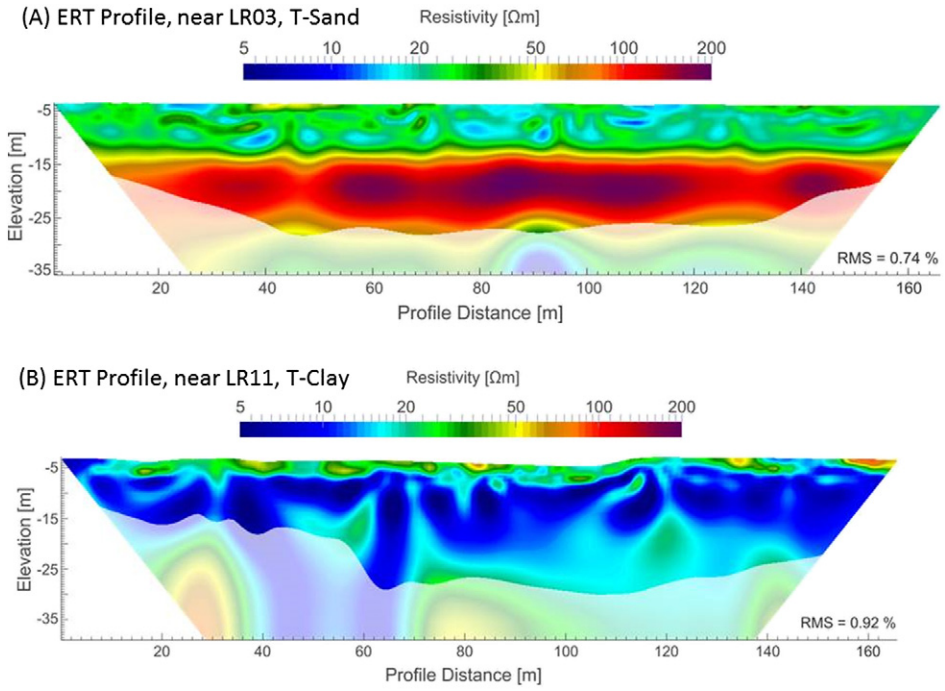

Fig. 2. Selected electrical resistivity tomography (ERT) profiles showing key differences in resistivity and inferred hydraulic conductivity at locations on (A) T-Sand and (B) T-Clay, near zones previously indicated by yellow boxes on Fig. 1A and B, respectively. The T-Clay ERT profile shows the majority of resistivity values are far below approximately 30 Ωm, indicating high clay content. In contrast, the T-Sand ERT profile shows only small lenses with low resistivity values, with the majority of data are above 30 Ωm, indicating that the sand content in T-Sand is likely to be significantly higher than in T-Clay. The ERT profiles suggest that T-Sand should have a much higher hydraulic conductivity in both shallow and deeper layers than expected at T-Clay. The small root-mean-square (RMS) misfit highlights the very good agreement between the measured and modelled data and indicates a high reliability of the resistivity profiles. ERT provided the basis for transect selection.

during sample collection. Sample collection began upon stabilization of *Eh* (typically the slowest multi-meter reading to stabilize) or after a maximum of pumping approximately 1.5 borehole volumes (Richards et al., 2015), whichever came first. *In-situ* analysis of sulfide, ammonium, nitrite, nitrate, iron, manganese, fluoride and orthophosphate was conducted immediately following sample collection using a field spectrophotometer (Spectroquant Nova 60A, Merck, Germany) and appropriate test kits (Table S1). The spectrophotometer general operation and wavelength accuracy was checked daily using PhotoCheck test set (Spectroquant PhotoCheck 14693, Merck, Germany) and standard solutions for each analyte were tested weekly during the pre-monsoon sampling campaign and the majority confirmed during the post-monsoon campaign (all standards from VWR, UK).

Subsamples of ground- and/or surface water were collected, filtered (0.45 μm cellulose and polypropylene syringe filters, Minisart RC, UK), and acidified to pH < 2 (trace grade nitric acid, BDH Aristar, UK) for analysis of cations using inductively coupled plasma atomic emission spectrometer (ICP-AES, Perkin-Elmer Optima 5300 dual view) (aluminum, barium, calcium, iron, lithium, magnesium, manganese, phosphorus, potassium, silicon, sulfur and strontium) and/or inductively coupled plasma mass spectrometry (ICP-MS, Agilent 7500cx) (arsenic, barium, cadmium, cerium, cobalt, copper, europium, lanthanum, lead, manganese, neodymium, selenium and strontium), both located within the Manchester Analytical Geochemistry Unit (MAGU) at The University of Manchester. Subsamples of un-acidified groundwater were collected and filtered (0.45 μm cellulose and polypropylene syringe filters, Minisart RC, UK) for analysis of anions (chloride, nitrite, nitrate, phosphate, fluoride, sulfate and bromide) using ion chromatography (IC; Dionex ICS5000 Dual Channel Ion Chromatograph) at MAGU. Dissolved organic carbon (DOC) was measured on subsamples filtered (0.45 μm glass microfiber syringe filters, Whatman/GE Healthcare, UK) and acidified to pH < 2 (trace grade nitric acid, BDH Aristar, UK) using a total organic carbon (TOC) analyzer (LABTOC TOC Analyzer, PPM, Netherlands) located at an UKAS accredited facility (Northumbrian Water Scientific Services, UK) for pre-monsoon samples and another TOC analyzer (Innovox Lab TOC Analyzer, GE, UK) located at ALS Environmental (UK) for post-monsoon samples. Samples collected for cation, anion and DOC analysis were stored in 100 mL glass Schott bottles which were acid-washed and furnaced before use. Alkalinity was measured on filtered (0.45 μm cellulose and polypropylene syringe filters, Minisart RC, UK) samples at MAGU using a visual titration kit (Aquamerck 111109, Merck, Germany) and confirmed with Gran Titration using 0.1 M HCl (analytical grade, Merck Millipore, UK) on selected samples. A correction factor of 0.9 was applied to the alkalinity measured using the test kit assuming the measured values are approximately a 10% overestimate (based on the gradient of the sum of anions *versus* sum of anions for all samples) likely arising from the relatively small titre volume (10 mL) used. For analytes measured using multiple methods (barium, manganese, strontium, iron, nitrite and nitrate), the following methods are preferred: ICP-MS for barium and strontium (for concentration range reasons); ICP-AES for manganese and iron (for concentration range reasons); and *in-situ* spectrophotometer for nitrite, nitrate and fluoride (for stability reasons).

The quality assurance/quality control measures undertaken typically included duplicate run analysis on ICP-AES, ICP-MS and IC analysis, with seven-point calibrations re-run every ten samples (Polya et al., 2017). The following certified reference materials (CRMs) were used: SRM 1640a (National Institute of Standards and Technology, USA) (National Institute of Standards and Technology, 2016); SRM 1643e (National Institute of Standards and Technology, USA) (National Institute of Standards and Technology, 2009); TM-25.2 (National Water Research Institute, Environment Canada); and SPS-SW1 (LGC Standards, UK) for ICP-MS and ICP-AES; TOC-WS (QC1308, Sigma-Aldrich, UK) for TOC; and NWBATTLE-02 and NWPERADE-09 (LGC Standards, UK) for IC. ICP-AES and ICP-MS calibration curves were calculated using inverse variance weighted first order linear models

(Polya et al., 2017; Miller and Miller, 2010). Corrections for drilling fluid contamination in groundwater samples were not made for major and trace inorganic analysis due to the typically low levels encountered (Richards et al., 2015). Data quality results are discussed in Section 3.2.

Subsamples for field-based arsenic speciation were collected using ion-exchange cartridges and methods previously developed (Watts et al., 2010). Ion-exchange cartridges were pre-conditioned to promote the adsorption of arsenic species. The resin-based strong cation-exchange cartridge (SCX, Bond Elut Jr. SCX, 12162040B, Agilent UK) was pre-conditioned using 15 mL 50% methanol (analytical reagent grade, VWR, UK) followed by 15 mL 1 M phosphoric acid (analytical reagent grade, VWR, UK) and 5 mL deionized water (RDI, Cambodia). The strong anion-exchange (SAX, Bond Elut Jr SAX, 12162044B) was preconditioned with 15 mL 50% methanol and 5 mL deionized water. Preconditioned cartridges were stored wet until use. A measured volume (30 mL) of ground- or surface water sample was passed through a 0.45 filter (0.45 μm cellulose and polypropylene syringe filters, Minisart RC, UK) into the SCX cartridge connected in series to an SAX cartridge. The filter removed particulate arsenic; the SCX cartridge retained DMA; the SAX cartridge retained As(V) and MA; and the effluent contained As(III). The effluent was stored in a 30 mL polyethylene bottle. Each of the cartridges and filter were detached, wrapped in sealing film (Parafilm, VWR, UK), and stored with the effluent bottle for each sample. At MAGU, the separate fractions were eluted as follows: (i) DMA was eluted from the SCX cartridge by 5 mL 1 M HNO_3^-; (ii) MA was eluted from the SAX cartridge by 5 mL 80 mL acetic acid; (iii) As(V) was subsequently eluted from the same SAX cartridge with 5 mL 1 M HNO_3^-. The eluted fractions were analysed for "total" arsenic by ICP-MS to determine the total arsenic present as each species. All water samples collected for further analysis were stored in the dark and refrigerated at approximately 4 °C until analysis.

2.4. Piezometric measurements

Piezometer levels were continuously logged at six sites (LR01, LR05, LR09, LR10, LR11 and LR14, located as shown on Fig. 1) from June 2014 until December 2015. The divers at LR01, LR09, LR10, LR11 and LR14 measured and recorded pressure and temperature (Mini-Diver, Schlumberger Water Services); the diver at LR05 measured and recorded pressure, temperature and electrical conductivity (CTD Diver, Schlumberger Water Services). An additional diver to allow for barometric pressure correction (Baro Diver, Schlumberger Water Services) was installed at LR11. All divers were installed at a depth of 10 m relative to the top of the well casing, with the exception of the barometric diver which was installed at a depth of 2 m (which was always above the water column). All data were recorded at 60 min intervals. Water level measurements were corrected for barometric pressure using Diver Office (Version 2012.1, Schlumberger Water Services). Local water level measurements were converted to absolute water levels using orthometric elevations (representing height above a theoretical sea level) measured at each site with high-accuracy GPS (C-Nav 3050 Dual Frequency & Glonass GPS receiver, antenna type NAV_ANT3001R, C-Nav, USA). Elevation measurements generally had a vertical accuracy of ±20 cm. In areas of relatively heavy vegetation (*e.g.* LR10, LR14) where vertical accuracy exceeded the tolerance of the C-Nav system, surveying was conducted using a total station (Leica Total Station TCR1205 R300). The WGS84 reference system was used. Surface water levels were provided by the Mekong River Commission from Monitoring Station Phnom Penh Chaktomuk (Bassac) (Mekong River Commission, 2015). Monitoring station data was adjusted to reflect the surface water levels of the Bassac and Mekong Rivers at the locations nearest the sampling sites by manual measurement. All piezometric measurements were calibrated to the Mekong River Commission data.

2.5. Geochemical modelling

Equilibrium speciation, model equilibrium electron activity (pe) of redox couples and mineral saturation indices were calculated using PHREEQC Interactive (Version 3.2.0.9820, 2015) and the minteq.v4.dat database (USGS, 2015). Groundwater inputs for each sample were temperature, pH, alkalinity (HCO_3^-), arsenic, calcium, magnesium, sodium, potassium, chloride, sulfate, iron, manganese, ammonium, nitrite, nitrate, barium, DO, fluoride, lithium, phosphate, strontium and sulfide. These parameters were selected for geochemical modelling as the key major, trace and redox-sensitive solutes relevant to the geochemical characteristics of these groundwaters and to the study's focus on understanding redox conditions and arsenic mobilization in shallow aquifers typical to Southeast Asia. Overall redox conditions were defined by field-measured *Eh* and converted to *Eh*-based electron activity (pe_{Eh}) using the Nernst equation (Appelo and Postma, 1993). The model pe of specific redox couples (*e.g.* ammonium/nitrite; ammonium/nitrate; nitrite/nitrate and DO/water), speciation and saturation indices were calculated directly by PHREEQC. When the model pe of a redox pair is relatively high, this means that the concentrations of the denominator species are relatively high compared to the numerator species; and *vice versa*, if the pe is relatively low, the concentrations of the denominator species are relatively low compared to the numerator species.

Hierarchical clustering analysis was undertaken with the PHREEQC model equilibrium pe outputs, using the Ward Linkages method *via* RGui (Version 2.14.3, 2013) (R Core Team, 2015) with installed packages caret (Kuhn et al., 2015), cluster (Maechler et al., 2015) and xlxs (Dragulescu, 2014). Imputation was used in the rare case of incomplete chemical analysis. All statistical analysis was completed using the statistical packages in OriginPro 2015. Regression statistics are reported with 95% confidence interval as $t(\textit{degrees of freedom}) = t\ value$; $p = p\ value$.

3. Results and discussion

3.1. Piezometric head variations

The groundwater level at each of the different transects displays distinct patterns in relation to the nearby surface water levels in the Bassac or Mekong Rivers (Fig. 3). For example, along T-Sand, the groundwater levels at site LR09 (within 400 m of the Bassac River) are well reflected in the surface water levels, both in terms of patterns and time suggesting ground-surface water hydraulic connectivity (Fig. 3A, marked with an arrow). At site LR10 on T-Clay (Fig. 3B), which is approximately 500 m from the Mekong River, the river patterns are also reflected, but with a dampened magnitude and a slight delay. Wells further from the river (*e.g.* LR05 and LR01 on T-Sand; and LR11 and LR14 on T-Clay) exhibit less seasonal variation. The observed patterns are in general agreement with previous studies showing that the groundwater flow direction in this area is heavily driven by seasonally-variable hydraulic gradients developed between the rivers and inland wetland basins (Polizzotto et al., 2008; Benner et al., 2008), and the similarities in patterns for T-Sand and T-Clay show the hydraulic symmetry of the inland basin between the Mekong and Bassac Rivers. Hydrographs extending beyond the period of post-monsoon water sampling (shown by the medium grey boxes on Fig. 3) show broadly similar trends in hydrological behaviour but different details and magnitudes of fluctuations. The hydraulic heads measured manually in each well along T-Sand and T-Clay (Fig. S2) are consistent with the hydrographs shown here and confirm the direction of groundwater flow, as inferred by observed gradients, is perpendicular to the river for both transects.

3.2. Analytical data quality

Analysis completed at MAGU was broadly in agreement with reported CRM values for analytes of key interest in both pre- and post-monsoon analytical batches, with calculated bias of weighted

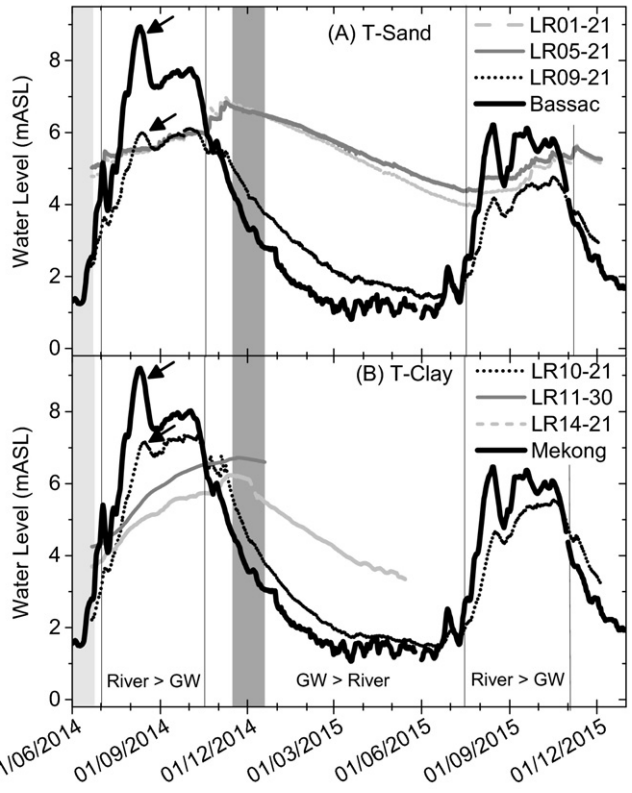

Fig. 3. Hydrographs of surface water compared to groundwater at major well clusters along (A) T-Sand and (B) T-Clay. The light and medium grey boxes represent the periods of pre- and post-monsoon water sampling campaigns, respectively. Solid vertical lines represent the approximate time when the surface water levels exceed those of the groundwater and *vice versa*. The wells closest to the rivers (*e.g.* LR09 on T-Sand and LR10 on T-Clay) exhibit strong seasonal variation, reflecting the changes observed in the surface waters. Wells further from the river (*e.g.* LR05 and LR01 on T-Sand; and LR11 and LR14 on T-Clay) exhibit less seasonal variation. Surface water levels for both the Mekong and Bassac were provided by the Mekong River Commission from the same Monitoring Station Phnom Penh Chaktomuk (Bassac) (Mekong River Commission, 2015), and were calibrated to the local water level measured nearest to T-Clay and T-Sand, respectively (measured offset between the Mekong and Bassac is approximately 25 cm). All groundwater data was calibrated with reference to the Mekong River Commission elevation datum at the Monitoring Station Phnom Penh Chaktomuk (Bassac) (Mekong River Commission, 2015).

calibration models within 10% of the CRM 1640a (Table S2) (National Institute of Standards and Technology, 2016). The errors reported for the concentration of individual elements (Table S5) determined using inverse variance weighted first order linear models take into account the analyte-dependent variance between calibration standards re-run typically every ten samples (Polya et al., 2017; Miller and Miller, 2010). Analysis of a prepared CRM dilution from the two TOC instruments used showed no difference exceeding analytical error of approximately 10%. Additionally, field measurements made using the spectrophotometer and appropriate test kits were generally in agreement with specifications of standard solutions (Table S3), however calculated biases were significant in some cases and dependent on concentration, analysis type, and field conditions (particularly temperature). Spectrophotometric analysis of procedural blanks sourced from locally available de-ionized water (Resources Development International, Cambodia) showed that all analytes were below detection limits. Photocheck solutions to test daily operation of the spectrophotometer were roughly consistent across both field campaigns (Fig. S3), however there were daily variations particularly for the lowest wavelength check solutions (445 nm), likely due to high temperatures above the range of recommended operation temperature and/or other local field conditions. It is expected this variability would have the largest influence on the reported concentration of analytes correspondingly measured at the lowest wavelengths (*e.g.* nitrate, low range nitrite and high range iron at 340 nm, 525 nm and 525 nm, respectively), at a level approximately commensurate with the magnitude of the greatest variability in check solution absorbance (*e.g.* a maximum of ~12%). Such variations in field conditions are difficult to control particularly in tropical climates away from infrastructure, although steps were made to reduce this impact (*e.g.* seeking shade for spectrophotometric analysis) when feasible.

An assessment of the overall degree of electroneutrality (Table S6) indicates that ground- and surface waters was typically within 10% (76% of samples are within 10% electroneutrality; 86% of samples are within 15% electroneutrality). The samples which exceeded 15% electroneutrality were variable in origin and depth, and are perhaps indicative of cumulatively large contributions of otherwise typically minor species and/or interferences with dissolved organic compounds (Tipping et al., 1991; Lydersen et al., 2004; Dudal and Gérard, 2004; Driscoll et al., 1994), although sampling, preservation or further analytical errors cannot be excluded.

3.3. High resolution profile of aqueous geochemistry

The major and trace elemental composition of the ground- and surface waters are summarized in Fig. 4. Groundwater chemistry is dominated by calcium and magnesium, constituting a maximum of 66% and 45%, respectively, of the bulk cationic charge, and bicarbonate, which contributes a maximum of 98% to the bulk anionic charge. Surface water is similarly dominated by calcium and magnesium (maximum 57% and 24%, respectively, of bulk cationic charge) and bicarbonate (maximum 80%). A Piper's diagram (Fig. S4) shows the dominant inorganic aqueous geochemistry and illustrates differences between T-Sand and T-Clay. Most groundwater samples were reducing (*Eh* range: −178–152 mV; median: −106 mV); circum-neutral (pH range: 6.6–8.4; median: 7.0) and around 30 °C (temperature range: 28.0–33.1 °C; median: 29.6 °C). Concentrations of dissolved arsenic in groundwaters range from 0.02 to 14.6 μM (2 to 1090 $\mu g \cdot L^{-1}$), with 93% of samples exceeding the World Health Organization (WHO) guideline value of 0.13 μM (10 $\mu g \cdot L^{-1}$) (World Health Organization, 2011) and 80% of them exceeding 0.67 μM (50 $\mu g \cdot L^{-1}$). Besides arsenic, the primary focus of this manuscript, most other groundwater constituents are below WHO guideline values for drinking water with the exception of (i) barium which exceeds the guideline of 5.1 μM (700 $\mu g \cdot L^{-1}$) in 17% of samples; (ii) nitrite which exceeds the guideline of ~0.7 mM (3 $mg \cdot L^{-1}$) in 49% of samples; and (iii) fluoride which exceeds the guideline of ~0.08 mM (1.5 $mg \cdot L^{-1}$) in 1% of samples (World Health Organization, 2011). The groundwater chemistry is typical of most arsenic-bearing groundwaters in Southeast Asia (Smedley and Kinniburgh, 2002; Lawson et al., 2013; Polizzotto et al., 2008; Polya et al., 2005; Rowland et al., 2008; Lawson et al., 2016; McArthur et al., 2001; Berg et al., 2001; Sovann and Polya, 2014; Buschmann and Berg, 2009; DPHE/MMI/BGS, 1999). Full summary statistics and sample-specific major and trace compositions (including electroneutrality) are provided in Supplementary Information (Tables S4, S5, and S6).

Arsenic concentrations vary significantly over both lateral and vertical spatial profiles, with higher concentrations generally observed in the deeper, sandy aquifers rather than in shallower, clay-dominated areas (Fig. 5). There is a strong overall correlation between arsenic and depth ($t(71) = 5.6$, $p = 4.7 \cdot 10^{-7}$), however there are exceptions to this trend in some cases. For example, relatively low arsenic (*e.g.* 0.2 μM) is observed at the deepest (45 m) well at site LR09 along T-Sand compared to shallower wells at the same location. This deviation may be due to the clay/silt deposit occurring at approximately 40 m depth and associated impacts on the hydrological and/or biogeochemical controls on arsenic mobilization or transport in this location (Harvey et al., 2002). The spatial distribution of arsenic in the horizontal

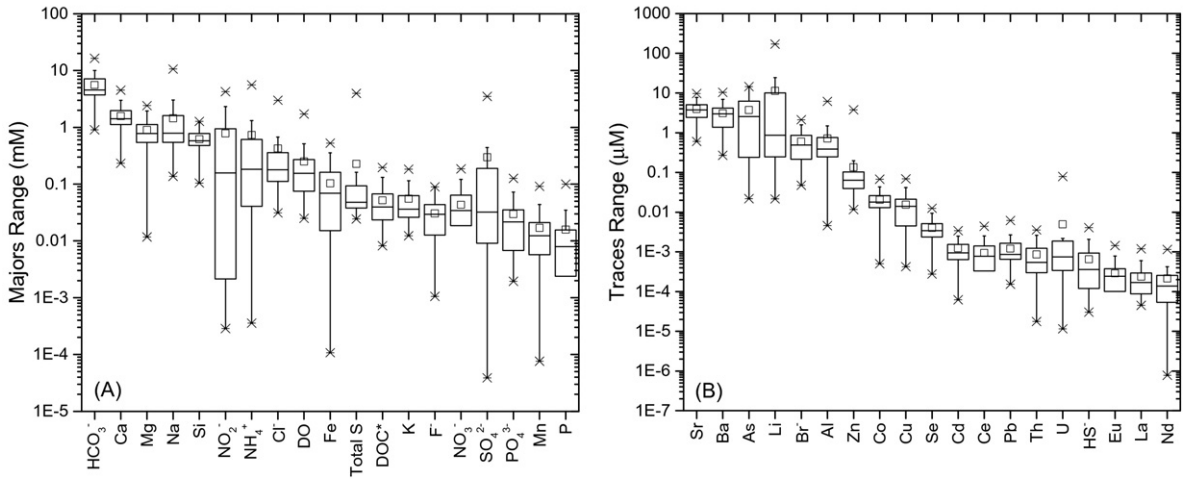

Fig. 4. Box chart representing summary statistics on a logarithmic scale of (A) major (mM) and (B) trace (μM) composition of Cambodian groundwater and surface water, arranged broadly in order of decreasing median concentration. Boxes represent the 25% and 75% range; the line within the box represents the median; the square represents the mean; the x represents the 1 and 99% range; and the straight lines indicate the maximum and minimum. Solutes were categorized as "trace" if the median concentration was less than approximately 10 μM. A Piper's diagram (Fig. S4) and further details are provided in Tables S4, S5, and S6.

direction is highly heterogeneous and there is no significant overall correlation between arsenic concentration and perpendicular distance from the Mekong or Bassac Rivers ($t(71) = -1.1$, $p = 0.29$). Arsenic concentrations at the same depth can vary as much as a factor of 4 along T-Sand (*e.g.* ranging from 2.1 to 8.6 μM at 21 m depth) or a factor of 5 along T-Clay (*e.g.* ranging from 2.6 to 14.6 μM at 21 m depth). The distribution of arsenic specifically along T-Clay (Fig. 5B) is consistent with previous correlations of arsenic concentrations, in part, with proximity to the Mekong River and associated permeability controls (Lawson et al., 2013; Kocar et al., 2008; Polizzotto et al., 2008). However, this explanation alone is not sufficient to explain the heterogeneity in arsenic concentrations observed along the new profile along T-Sand and the hydrological controls appear to be strongly contrasting in the two transects.

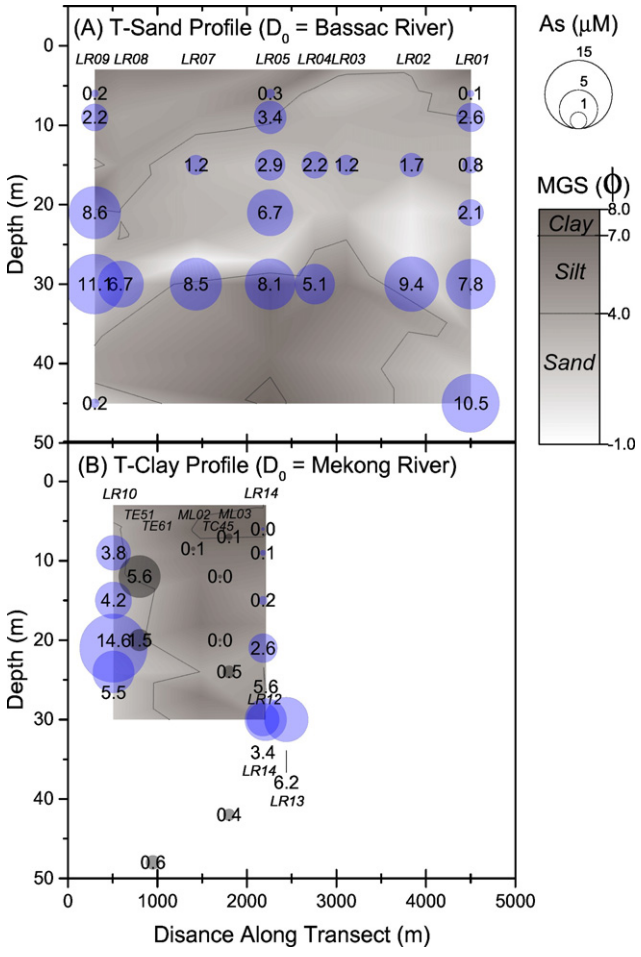

Fig. 5. The spatial distribution of pre-monsoon arsenic concentrations (μM) across (A) T-Sand and (B) T-Clay, with increasing distance from the Bassac and Mekong Rivers, respectively. Data from previous work by Lawson et al. (2013) is included on T-Clay to infill areas of limited spatial resolution and is shown in grey bubbles. The underlying contour represents the mean grain size (MGS) in sediments collected from the same locations within the aquifer, with darker colors representing smaller mean particle size.

Although the highest arsenic concentrations generally appear to occur in areas of aquifer sands (Fig. 5), the direct correlation of arsenic with the corresponding sedimentary φ (mean) *at the same depth* is generally poor (Fig. S5). For T-Sand there is no statistically significant correlation observed ($t(22) = -0.34$; $p = 0.736$, >0.05), however there is a significant correlation on T-Clay ($t(9) = -2.77$, $p = 0.022$, <0.05). These different correlations for the two transects are attributed to the sedimentological heterogeneity and depositional history of the area, which means that the mean grain size at, say, 30 m on T-Sand may be different to that at 30 m in another location on T-Clay. This is not inconsistent with the strong overall correlation with arsenic and depth (Fig. 5), but rather illustrates that grain size alone may not be sufficient to explain the aqueous arsenic concentrations. This suggests that the controls on aqueous arsenic concentrations are complex and vary in different locations, and may be affected by factors such as lithology, hydrological controls, biogeochemical conditions, partial equilibrium conditions, and/or competing near-surface *versus* in-aquifer processes (Lawson et al., 2013; Kocar et al., 2008; Polizzotto et al., 2008; Lawson et al., 2016).

The lateral and vertical profiles of sulfate, iron and DO are consistent with the variation of arsenic (Fig. 6). Arsenic concentrations in the groundwater are broadly inversely correlated with sulfate in both transects ($t(70) = -2.60$, $p = 0.01$), with the highest concentrations of sulfate observed (*e.g.* ~3.5 mM at site LR14) in relatively shallow, low arsenic groundwaters. In these high sulfate groundwaters the geochemical conditions are not favorable to support sulfate reduction. The drastic changes particularly in sulfate concentration with depth suggest the presence of differing redox zones across the field sites. Arsenic and DO are also inversely correlated ($t(71) = -2.64$, $p = 0.01$). In contrast to the inverse correlation observed between arsenic and sulfate and DO, arsenic and iron

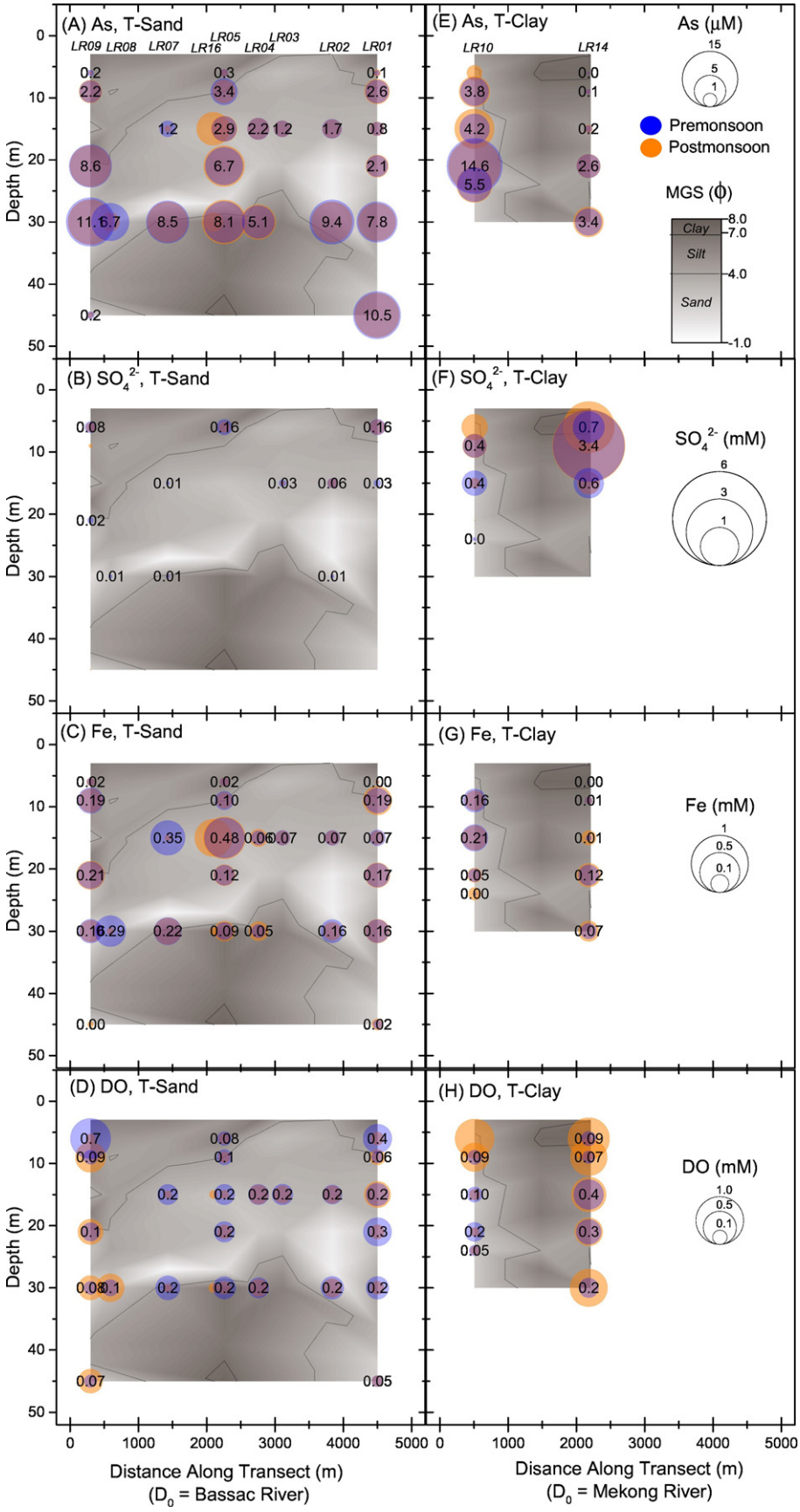

Fig. 6. Spatial profile of (A & E) arsenic; (B & F) sulfate; (C & G) iron; and (D & H) dissolved oxygen (DO) across T-Sand (left) and T-Clay (right), which are broadly perpendicular to the Bassac and Mekong Rivers respectively. Labelled datapoints represent pre-monsoon concentrations (blue bubbles) and post-monsoon concentrations (orange bubbles) are unlabelled. Values on T-Clay are shown only for the two major well nests LR10 and LR14 for clarity. The underlying contour represents the mean grain size (MGS) in sediments at the same depth as the water sample, with darker colors representing smaller mean particle size.

are positively correlated in both transects ($t(71) = 2.02$; $p = 0.05$). Elevated concentrations of arsenic and iron in reducing conditions is consistent with the reductive dissolution of iron (hydr)oxides mechanism of arsenic mobilization as well as with previous studies in this area (Islam et al., 2004; Lawson et al., 2013; Kocar et al., 2008; Lawson et al., 2016).

Significant seasonal variations in groundwater composition are noted for some sites (*e.g.* LR09, LR10 and LR14). The strongest observed changes at LR09 along T-Sand in post-monsoon samples include a decrease in DO and sulfate at 6 m followed by an increase in DO at depths 9 m and greater. This suggests rapid incursion of Bassac River water during the monsoon season, which is consistent with the strong similarities in flow patterns observed between the Bassac River and the groundwater level in LR09 (Fig. 3A). There are also monsoonal changes in DO and sulfate observed on T-Clay at LR10 (closest to the Mekong River) and LR14 (near a wetland pond). These patterns are indicative of ground-surface water interactions driven by monsoonal patterns, and are consistent with the modelled provenance of recharge sources based on stable isotope mixing models at these sites (Richards et al., 2017).

The spatial and seasonal distribution of nitrogen-containing compounds nitrite, nitrate and ammonium (Fig. 7) are consistent with the reducing conditions prevailing in this arsenic-bearing groundwater and provide further support of seasonal changes in groundwater geochemistry at certain locations. The low concentrations of nitrate coupled with elevated concentrations of nitrite are consistent with the reducing conditions. Elevated concentrations of ammonium are noted in places in relatively close proximity to surface water sources and/or sandy lithology and may be indicative of ground-surface water interactions. Seasonal changes in redox conditions at several sites (*e.g.* LR09, LR10, LR14) are consistent with changes observed in other geochemical parameters (*e.g.* sulfate and DO as on Fig. 6) as well as stable isotope-based mixing models (Richards et al., 2017), and are indicative of rapid influx of surface water to the aquifer system during the monsoonal season. These data suggest the presence of sensitive, heterogeneous redox zones which are seasonally-dependent and affect aquifer chemistry.

Although seasonal changes are noted for some sensitive redox parameters, pre- and post-monsoon arsenic concentrations (Fig. S6) are typically very similar and strongly correlated ($t(33) = 16.4$; $p < 0.001$). A limited number of samples (*e.g.* LR10-15, LR08-30 and LR07-15) show seasonal variation in arsenic concentration which is significantly greater than ~10%. Interestingly, the pre-monsoon arsenic at site LR10-15 is approximately half of the post-monsoon value; an observation which can be linked with a significant postmonsoonal decrease in sulfate and increase in ammonium at this location (Figs. 6F and 7F, respectively). Similarly, the seasonal changes in arsenic concentration at LR08-30 and LR07-15 are also reflected in seasonal changes in iron, DO (Fig. 6C and D, respectively), nitrite and ammonium (Fig. 7A and C, respectively). These site-specific seasonal trends help to identify zones where geochemical conditions (including arsenic concentration) may change rapidly on very short, seasonal time scales. Further evaluation of the potential impacts of seasonal surface water ingression on arsenic mobilization and transport is warranted and may be important in predictions of seasonal and/or secular changes in arsenic hazard.

3.4. Arsenic speciation

The *in-situ* speciation of arsenic (Fig. S7 and Table S7) shows that As(III) is the dominant arsenic species in most samples, with As(III) comprising of >80% of the sum of the arsenic species in 90% of the samples. In the few cases where As(III) is <80% of the sum of the arsenic species, the As(V) fraction is more substantial or even dominant in shallow samples (*e.g.* LR10-6-POST and LR14-6-POST which are 74% and 28%, respectively) which are also characterized by high DO and oxidizing (in the case of LR14-6-POST) or only very slightly reducing conditions (in the case of LR10-6-POST). Concentrations of organic arsenic forms (DMA and MMA) were generally very low, as typically expected in groundwaters (Chen et al., 1995), but still present in some samples. For example, MMA was >10% of the sum of the arsenic species in the shallow samples LR10-6-POST (22% or 0.09 μM MMA). The presence of these organic species can be caused as a result of methylation reactions catalysed by bacteria or algae (Smedley and Kinniburgh, 2002) which could be expected due to the shallow nature of these samples, sandy lithology and close proximity to surface water sources at both sites. Recoveries (defined as the sum of arsenic species eluted from ion exchange cartridges divided by total arsenic) were in the acceptable range of 80–120% recovery in 78% of the samples, however recoveries ranged from 14% to 566% (median 91%). Factors contributing to poor recoveries in some cases may include competition with other ions on the ion exchange resin (which would likely result in recoveries <100%), incomplete pre-conditioning or elution of cartridges, other matrix effects influencing sorption and/or analysis (Watts et al., 2010), and/or field sampling or analytical error (which could potentially either lead to recoveries <100% or >100% depending on the circumstance; unfortunately such errors are difficult to trace given field constraints and limited sample volume). Matrix effects are likely to be complex and there was no statistically significant relationship between recovery and iron concentration ($t(32) = -1.41$, $p = 0.168$, >0.05) nor electrical conductivity ($t(32) = 0.099$, $p = 0.921$, >0.05). The dominance of As(III) and generally high As(III)/$\sum$As Species ratios (>80%) in most samples is expected from the generally reducing groundwater chemistry and has been confirmed using PHREEQC geochemical speciation modelling in a sub-set of representative groundwaters (Table S8). Parameters for geochemical modelling of organic arsenic species MMA and DMA are not available using PHREEQC and minteq.v4.dat database.

3.5. Identification of key redox zones

To further understand the sensitive redox chemistry in these aquifers, speciation modelling has been conducted to identify the model pe of key redox pairs (*e.g.* ammonium/nitrite; ammonium/nitrate; nitrite/nitrate; and DO/water) (Table S9). Using hierarchical clustering algorithms (R Core Team, 2015; Kuhn et al., 2015; Maechler et al., 2015; Dragulescu, 2014), the redox couples have been clustered into four key redox groups or zones of broadly similar characteristics which can be visualized with model pe-pH diagrams (Fig. 8). The general and relative characteristics of each redox zone are listed for reference (Table 2). Generally Zone 1, representing relatively high pe (NH_4^+/NO_2^-), pe (NH_4^+/NO_3^-), pe (DO/O_2^-), and low pe (NO_2^-/NO_3^-) activity, is dominant in near-surface to mid aquifer areas. This near-surface zone sits above deeper redox zones (*e.g.* Zones 2, 3 and 4) which are generally marked by lower redox pair activities.

The redox classifications proposed here reflect the local groundwater geochemistry and provide more detail for these specific conditions than previous classifications (Bjerg et al., 1995; Christensen et al., 2000; Baedecker and Back, 1979; Lyngkilde and Christensen, 1992), commonly used to describe landfill leachates or other generic contaminant plumes. As noted by Christensen et al. (2000), no universally accepted procedures exist for the determination of redox conditions, however the presence of differing redox-sensitive compounds are general indicators of differing redox conditions. Some typical indicators include: (i) the presence of Fe(II) and Mn(II), which were expected in every groundwater sample, indicating anaerobic conditions and iron and manganese reduction, respectively; (ii) typically lower concentrations of DO, as were observed with increasing depth (Fig. 6D and H) indicating anaerobic conditions; and (iii) the presence of nitrate (which in these groundwaters was always less than ~0.2 mM as shown on Fig. 7C and D) indicating aerobic or nitrate reducing conditions (Christensen et al., 2000).

The four redox zones help visualize changes in redox conditions with transect, depth, site (Fig. 9) and season (Fig. 10). The electron activity of ammonium/nitrite and ammonium/nitrate couples generally decrease with depth at a particular site, reflecting the

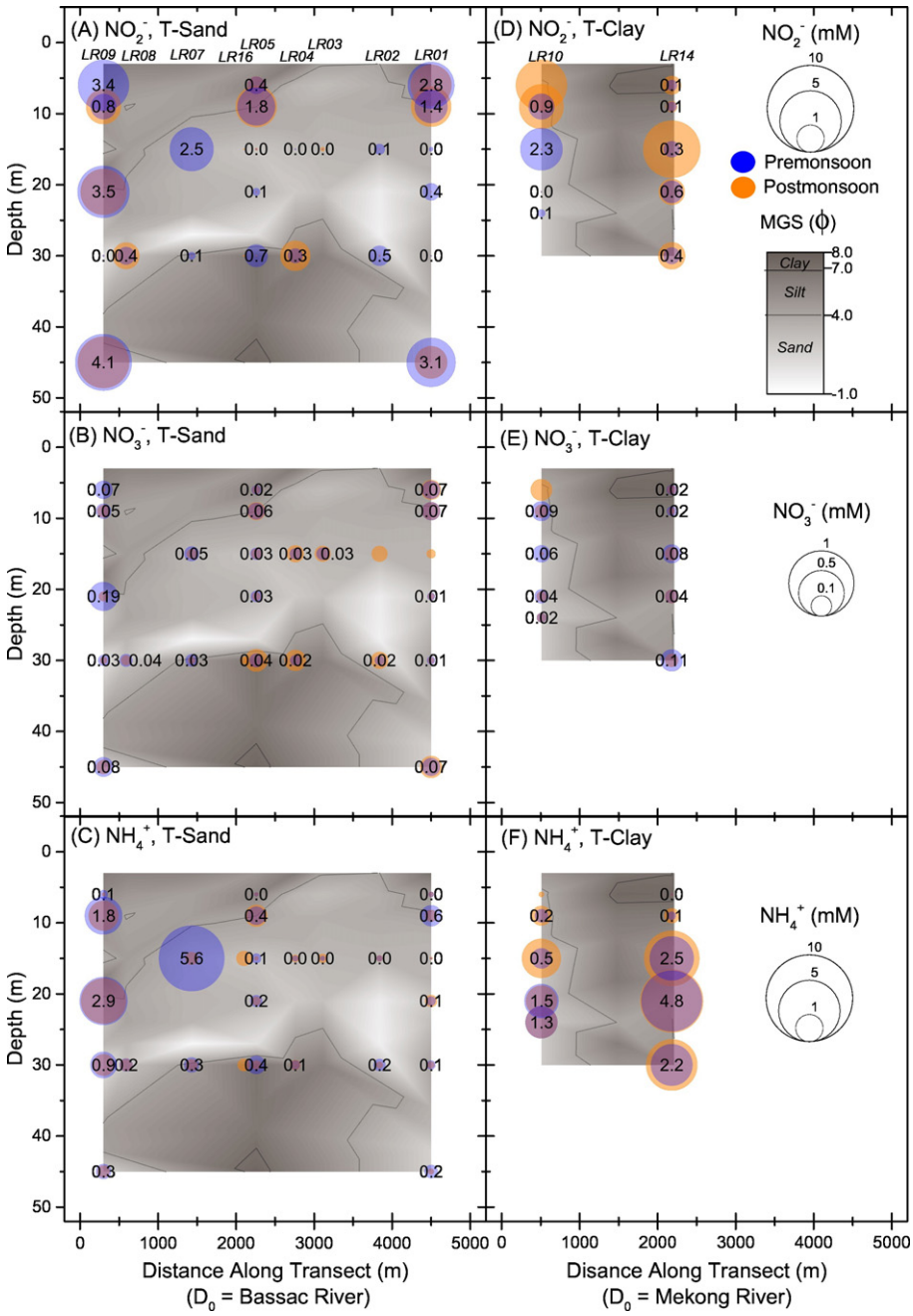

Fig. 7. Spatial distribution of nitrogen-containing components (A & D) nitrite; (B & C) nitrate; and (C & F) ammonium in groundwaters during the pre-monsoon (blue; values reported) and post-monsoon (orange) season. Note the bubbles sizes are on different scales for clarity.

more reducing conditions typically encountered at depth. The electron activity of nitrite/nitrate couples generally reaches a maximum mid-aquifer followed by a decrease at the deepest samples. The DO/water couples tend to show a decrease with depth, with the exception of site LR14, where this ratio does not significantly change or is variable with depth.

The redox zones shift and become more variable post-monsoon as compared to pre-monsoon (Fig. 10), which can be attributed to rapid ingression of surface water into the aquifer system in certain locations during the monsoon season (such as near rivers as in LR09 and LR10, where there is sand-dominance such as LR10 and LR05, or where sites are in close proximity to ponds such as LR05). These changes are consistent with the specific geochemical data presented (Figs. 6 and 7) as well as the modelled provenance of recharge sources using stable isotope-based mixing models in this field area (Richards et al., 2017). In site LR01, for example, the boundary between Zone 1 and Zone 2 increases on the order of 10 m post-monsoon; and a similar change is noted in LR09. The redox conditions in LR09 become much more variable post-monsoon which may be attributed to interactions with the nearby Bassac River. Similarly, at site LR14, a single redox zone dominates the entire depth profile pre-monsoon, however another zone appears (at variable depths) post-monsoon. This site is in very close proximity to site ML04 in a previous study where tritium was found at depth and attributed to pond-derived interactions (Lawson et al., 2013). At site LR10, the post-monsoon samples have the same general redox zones as pre-monsoon, but the depths are shifted upwards post-monsoon reflecting

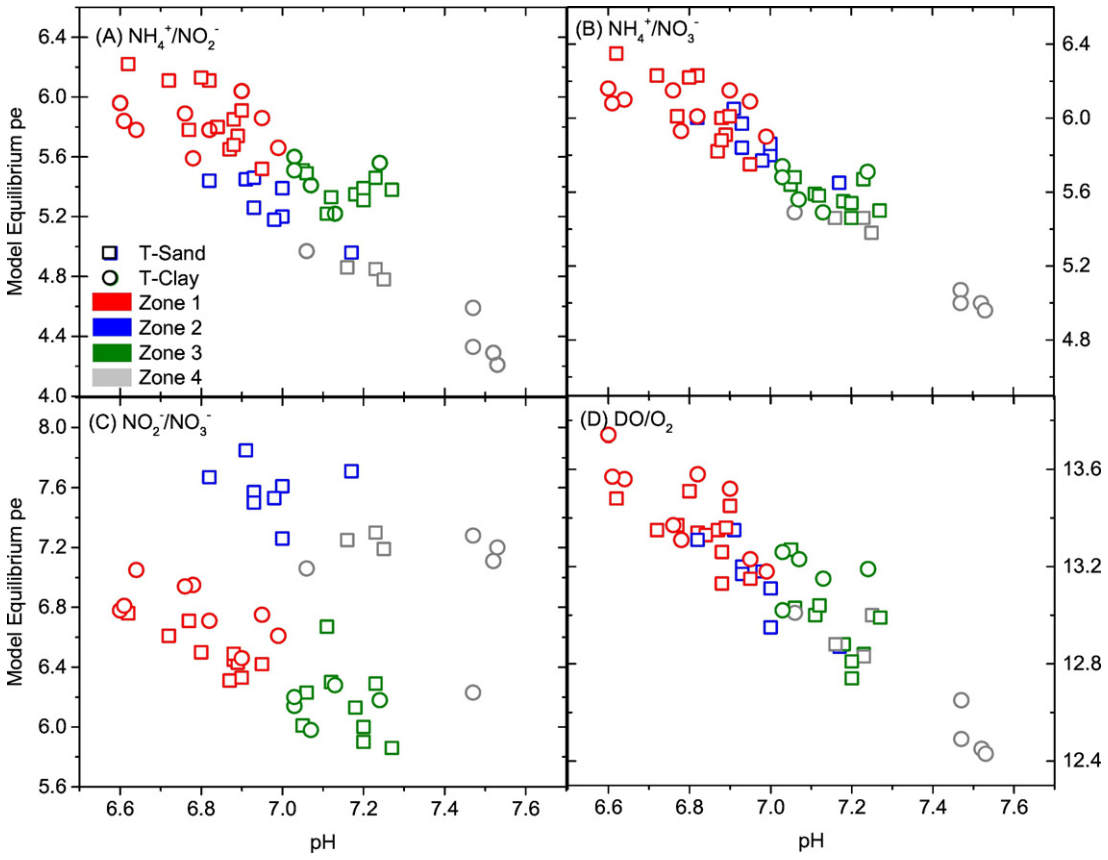

Fig. 8. Model equilibrium pe-pH diagram of measured concentrations of key redox pairs (A) NH_4^+/NO_2^-; (B) NH_4^+/NO_3^-; (C) NO_2^-/NO_3^- and (D) DO/O_2 at the major clusters along T-Sand and T-Clay. Color groups represent redox groups of broadly similar characteristics.

the higher water table. Interestingly there is a significant change in arsenic concentration noted at LR10-15, with higher arsenic concentration in the post-monsoon sample (Fig. S6). The higher post-monsoon arsenic noted at LR10-15 is consistent with the post-monsoonal up-shifting of Zone 4 and the higher arsenic concentrations found at depth at site LR10. These spatial and temporal shifts in redox zones illustrate the fluidity of the groundwater geochemistry. It is important to note that these zones do not represent the occurrence of a single redox process per zone, but rather groupings of similar redox parameters where overlapping processes and complex and/or partial redox reactions are likely (Mukherjee et al., 2008; Jakobsen and Postma, 1999).

3.6. Mineral saturation indices

Saturation index calculations for pre-monsoon groundwater at the major well clusters (Table S10) show that groundwater is generally near equilibrium with respect to key carbonate-hosting phases such as calcite, siderite and dolomite although the relatively high levels of HCO_3^- observed in some groundwater samples cannot be fully attributed to carbonate dissolution; thus there may likely be contributions from other sources such as oxidation of organic matter (Mukherjee et al., 2008; Ahmed et al., 2004). The characterization including provenance of organic matter in this system is the subject of ongoing work. Groundwater is supersaturated with the key Fe(III) and mixed Fe(II)/Fe(III) phases goethite, hematite, magnetite, and slightly undersaturated with ferrihydrite. The principle aqueous species of iron is Fe(II) and there is no significant complexation of iron with other inorganic components. The supersaturation of pyrite in 12 samples (43% of samples) indicates that the conditions (*e.g.* sufficiently reducing and sufficient concentrations of total iron and sulfate) are favourable in those locations to support sulfate reduction and possible sulfide precipitation. Because the groundwater is supersaturated with the key Fe(III) and mixed Fe(II)/Fe(III) phases, there should be sufficient iron available to form pyrite if the conditions were favourable; that pyrite is not formed in a number of samples suggests that the *Eh* of the groundwater remains too high to support sulfate reduction in those places. This is consistent with the sulfate data presented on Fig. 6. With the exception of barium arsenate, groundwater at all wells is highly undersaturated with the major arsenic oxide/oxyanion phases (*e.g.* scorodite, arsenolite and arsenic pentoxide), indicating that arsenic should generally remain

Table 2
Characteristics of key redox zones identified by hierarchical clustering of the activities of the following redox couples: ammonium/nitrite; ammonium/nitrate; nitrite/nitrate; and dissolved oxygen/water. The (value) indicates the maximum model pe in the zone for the appropriate redox pair and the qualitative comparisons relate to the various zones for a given redox pair.

Redox zone	% of samples	Color code	pe (NH_4^+/NO_2^-)	pe (NH_4^+/NO_3^-)	pe (NO_2^-/NO_3^-)	pe (DO/O_2)
Zone 1	40%	Red	High (6.2)	High (6.4)	Low (7.1)	High (13.7)
Zone 2	15%	Blue	Low (5.5)	Med (6.1)	High (7.9)	Med (13.4)
Zone 3	29%	Green	Med (5.7)	Low (5.7)	VLow (6.7)	Low (13.3)
Zone 4	15%	Grey	VLow (5.0)	VLow (5.5)	Med (7.3)	VLow (13.0)

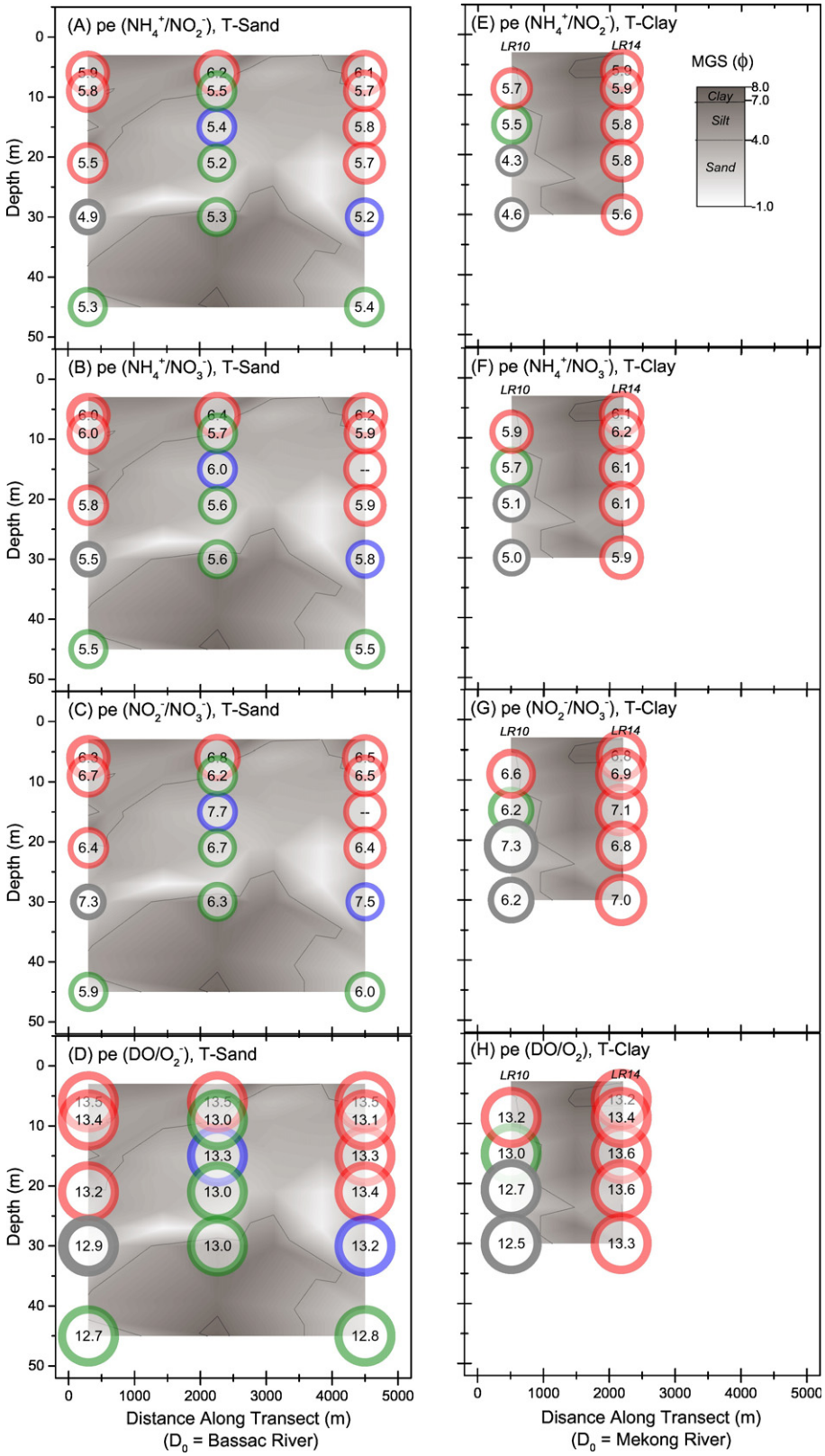

Fig. 9. Model equilibrium pe of measured concentrations of key redox pairs (ammonium/nitrite; ammonium/nitrate; nitrite/nitrate; dissolved oxygen/water) in pre-monsoon samples. Colors indicate redox zone (Zone 1: Red; Zone 2: Blue; Zone 3: Green; Zone 4: Grey) as defined in Table 2 and Fig. 8.

dissolved after mobilization (Mukherjee et al., 2008). The minor arsenic phase barium arsenate is supersaturated in most samples. The arsenic-sulfur species orpiment is supersaturated in a number of samples but realgar is highly undersaturated.

Three paired pre- and post-monsoon mineral saturation indices have been included (Table S10) for samples where a shift in redox zone is observed after the monsoon season (Fig. 10). For each of these three sets, changes in saturation indices are observed, reflecting the

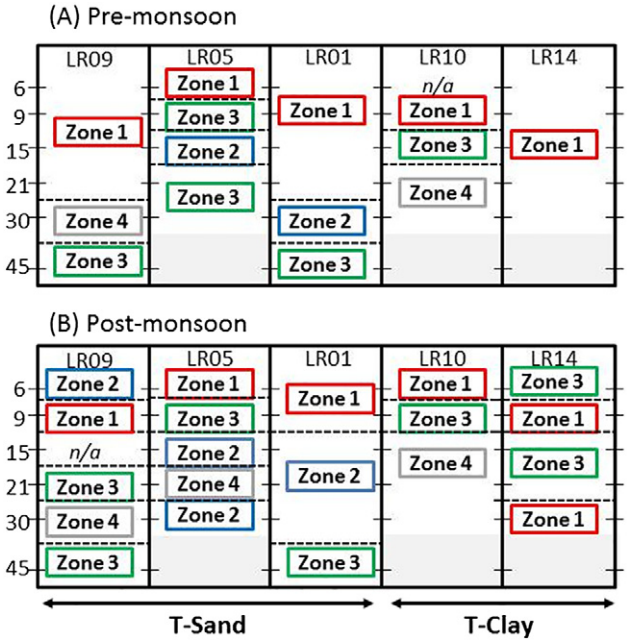

Fig. 10. Key redox zones for the five major well clusters (LR09, LR05, LR01, LR10, LR14) under pre- and post-monsoon conditions. Zones were determined using hierarchical clustering of the model equilibrium pe of measured concentrations of the following redox couples: ammonium/nitrite; ammonium/nitrate; nitrite/nitrate; and dissolved oxygen/water.

changing aquifer geochemistry. In most cases, these changes do not reflect a change in overall saturation. However, pyrite, which is supersaturated in each of these three samples pre-monsoon, is undersaturated during post-monsoon conditions along T-Sand (sulfide was not detected in these samples). This snapshot supports that saturation conditions within the aquifer change on a seasonal basis in certain locations. The saturation indices of calcite, siderite, dolomite and goethite across the major clusters in T-Clay and T-Sand (Fig. S8) show changes with depth and transect as well as the relatively strong seasonal changes observed with goethite (as was observed with hematite and magnetite, data not shown) in T-Clay.

4. Conclusions

A high resolution network of well clusters has been installed in a heavily arsenic-affected aquifer in northern Kandal Province, Cambodia, to monitor changes in groundwater chemistry along key groundwater flow paths in two distinct transects. Groundwater concentrations of arsenic are highly heterogeneous vertically (with changes monitored on the order of 3 to 15 m in depth) and laterally on the order of several hundred meters. Changes in arsenic concentration cannot be sufficiently explained by relatively simple proxies such as the mean grain size of the hosting sediment or proximity from the nearby Mekong and/or Bassac Rivers. High arsenic concentrations across the transects are generally associated with reducing conditions with relatively high concentrations of iron, and relatively low concentrations of sulfate and DO, which is consistent with the arsenic mobilization mechanism caused by reductive-dissolution of iron (hydr)oxides. Key redox zones have been identified using groupings of major redox couples (ammonium/nitrite; ammonium/nitrate; nitrite/nitrate; dissolved oxygen/water), and redox zones shift with depth, site and season. Seasonal changes in groundwater chemistry are attributed to surface-groundwater interactions driven by monsoonal patterns and are consistent with the separate provenance of recharge sources using stable isotope-based mixing models. Surface-groundwater interactions tend to occur in areas which are (i) sandy and high permeability (*e.g.* T-Sand); (ii) in close proximity to rivers (*e.g.* LR09, LR10); and/or (iii) in close proximity to ponds (*e.g.* LR14). Future age-based and isotopic determinations of groundwaters, surface waters and sediment will help to provenance the source, age, potential mixing regimes and subsequent controls on aquifer chemistry, and detailed organic characterization will assist in identifying the controls on the organic matter implicated in arsenic release under these conditions.

Acknowledgements

This research was funded by a NERC Standard Research Grant (NE/J023833/1) to DP, BvD and CB, a NERC PhD studentship (NE/L501591/1) to DM and additional support from the Leverhulme Trust (ECF2015-657) to LR. We are extremely grateful for the generous contributions of our hardworking local drilling team led by Hok Meas, the field assistants during our water sampling campaigns (Pheary Meas, Teyden Sok and Yut Yann from the Royal University of Agriculture, Cambodia, and Chhengngunn Aing and Zongta Sang from the Royal University of Phnom Penh, Cambodia), and the field assistants during the geophysical campaigns (Vichet Hang, Sereyrath Aing, Borey Horm, Savuth Yim, Chhengngunn Aing, Sitha Sean and Zongta Sang, all Royal University of Phnom Penh). Helen Downie (The University of Manchester, UK), Lee Chambers (The University of Lancaster, UK), and Lucy Oxby (British Geological Survey, UK) are also thanked for their contribution to field work. Ann Hall, Marc Hall, Lori Frees, Lori Allen and Dina Kuy (Resources Development International – Cambodia, RDI) are thanked for logistical support and the usage of laboratory facilities at RDI. Paul Lythgoe and Alastair Bewsher (both The University of Manchester) are thanked for analytical support for ICP and IC analysis, respectively, and Northumbrian Water Scientific Services for conducting TOC analysis. Ahmed Ali Nassir Al Bualy (The University of Manchester) is thanked for assistance with calibration modelling. Gren Turner and Barry Rawlins (British Geological Survey) and Lee Chambers are thanked for advice, analytical support and/or assistance with sediment particle size measurements. Merren Jones (The University of Manchester) is thanked for useful discussions regarding sedimentology and Gillian Lord (University of Surrey, UK) for useful discussions regarding field methods for arsenic speciation. Julien Declercq, Andrew Barnes and David Tait (all SRK Consulting, UK) are thanked for their advice to LR on geochemical modelling. The contributions of SU and OK are published with the permission of the Executive Director of the British Geological Survey (NERC). We thank the three anonymous reviewers for their comments which have significantly improved the clarity of the manuscript.

Appendix A. Supplementary data

Supplementary data to this article can be found online at http://dx.doi.org/10.1016/j.scitotenv.2017.02.217.

References

Ahmed, K.M., et al., 2004. Arsenic enrichment in groundwater of the alluvial aquifers in Bangladesh: an overview. Appl. Geochem. 19, 181–200.
Al Lawati, W.M., et al., 2012. Characterisation of organic matter and microbial communities in contrasting arsenic-rich Holocene and arsenic-poor Pleistocene aquifers, Red River Delta, Vietnam. Appl. Geochem. 27, 315–325.
Al Lawati, M.M., et al., 2013. Characterisation of organic matter associated with groundwater arsenic in reducing aquifers of southwestern Taiwan. J. Hazard. Mater. 262, 970–979.
Appelo, C.A.J., Postma, D., 1993. Geochemistry, Groundwater and Pollution (Balkema).
Baedecker, M.J., Back, W., 1979. Hydrogeological processes and chemical reactions at a landfill. Groundwater 17 (5), 429–437.
Balzer, W., 1982. On the distribution of iron and manganese at the sediment/water interface: thermodynamic versus kinetic control. Geochem. Cosmochim. Acta 46 (7), 1153–1161.
Benner, S.G., et al., 2008. Groundwater flow in an arsenic-contaminated aquifer, Mekong Delta, Cambodia. Appl. Geochem. 23 (11), 3072–3087.
Berg, M., et al., 2001. Arsenic contamination of groundwater and drinking water in Vietnam: a human health threat. Environ. Sci. Technol. 35 (13), 2621–2626.
Bhattacharya, P., Chatterjee, D., Jacks, G., 1997. Occurence of arsenic contaminated groundwater in alluvial aquifers from delta plains, eastern India: options for safe drinking water supply. Water Resour. Dev. 13, 79–92.

Bjerg, P.L., et al., 1995. Distribution of redox-sensitive groundwater quality parameters downgradient of a landfill (Grindsted, Denmark). Environ. Sci. Technol. 29, 1387–1394.

Blott, S.J., Pye, K., 2001. GRADISTAT: a grain size distribution and statistics package for the analysis of unconsolidated sediments. Earth Surf. Process. Landf. 26, 1237–1248.

Borch, T., et al., 2010. Biogeochemical redox processes and their impact on contaminant dynamics. Environ. Sci. Technol. 44, 15–23.

Buschmann, J., Berg, M., 2009. Impact of sulfate reduction on the scale of arsenic contamination in groundwater of the Mekong, Bengal and Red River deltas. Appl. Geochem. 24 (7), 1278–1286.

Charlet, L., Polya, D.A., 2006. Arsenic in shallow, reducing groundwaters in southern Asia: an environmental health disaster. Elements 2, 91–96.

Chen, W.-F., Liu, T.-K., 2003. Dissolved oxygen and nitrate of groundwater in Choshui Fan-Delta, western Taiwan. Environ. Geol. 44, 731–737.

Chen, S.L., et al., 1995. Trace element concentration and arsenic speciation in the well water of a Taiwan area with endemic Blackfoot disease. Biol. Trace Elem. Res. 48, 263–274.

Cherry, J.A., et al., 1979. Arsenic species as an indicator of redox conditions in groundwater. J. Hydol. 43, 373–392.

Christensen, T.H., et al., 2000. Characterization of redox conditions in groundwater contaminant plumes. J. Contam. Hydrol. 45, 165–241.

Datta, S., et al., 2011. Perennial ponds are not an important source of water or dissolved organic matter to groundwaters with high arsenic concentrations in West Bengal, India. Geophys. Res. Lett. 38 (L20404).

van Dongen, B., et al., 2008. Hopane, sterane and n-alkane distributions in shallow sediments hosting high arsenic groundwaters in Cambodia. Appl. Geochem. 23, 3047–3058.

DPHE/MMI/BGS, 1999. Groundwater studies for arsenic contamination in Bangladesh. Rapid Investigation Phase Final Report.

Dragulescu, A., 2014. R Package 'xlsx' (Version 0.5.7): Read, Write, Format Excel 2007 and Excel 97/2000/XP/2003 Files. https://cran.r-project.org/web/packages/xlsx/xlsx.pdf, last accessed 20 October 2015.

Driscoll, C.T., Lehtinen, M.D., Sullivan, T.J., 1994. Modeling the acid-base chemistry of organic solutes in Adirondack, New York, lakes. Water Resour. Res. 30 (2), 297–306.

Dudal, Y., Gérard, F., 2004. Accounting for natural organic matter in aqueous chemical equilibrium models: a review of the theories and applications. Earth Sci. Rev. 66, 199–216.

Gulens, J., Champ, D.R., Jackson, R.E., 1978. Influence of redox environments on the mobility of arsenic in groundwater. In: Barry, P.J. (Ed.), Hydrological and Geochemical Studies in the Perch Lake Basin: A Second Report of Progress (AECL-6404). Atomic Energy of Canada Limited, p. 223.

Harvey, C.F., et al., 2002. Arsenic mobility and groundwater extraction in Bangladesh. Science 298, 1602–1606.

Islam, F.S., et al., 2004. Role of metal-reducing bacteria in arsenic release from Bengal delta sediments. Nature 430, 68–71.

Jakobsen, R., Postma, D., 1999. Redox zoning, rates of sulfate reduction and interactions with Fe-reduction and methanogenesis in a shallow sandy aquifer, Rømø, Denmark. Geochim. Cosmochim. Acta 63 (1), 137–151.

Kocar, B.D., et al., 2008. Integrated biogeochemical and hydrologic processes driving arsenic release from shallow sediments to groundwaters of the Mekong delta. Appl. Geochem. 23 (11), 3059–3071.

Kuhn, M., et al., 2015. Caret: Classification and Regression Training (Version 6.5-57). https://github.com/topepo/caret/, last accessed 20 October 2015. (Available from: https://github.com/topepo/caret/).

Lawson, M., et al., 2013. Pond-derived organic carbon driving changes in arsenic hazard found in Asian groundwaters. Environ. Sci. Technol. 47, 7085–7094.

Lawson, M., et al., 2016. Tracing organic matter composition and distribution and its role on arsenic release in shallow Cambodian groundwaters. Geochim. Cosmochim. Acta 178, 160–177.

Lee, J.-J., et al., 2008. Delineation of spatial redox zones using discriminant analysis and geochemical modelling in arsenic-affected alluvial aquifers. Hydrol. Process. 22, 3029–3041.

Loke, M.H., Barker, R.D., 1995. Least-squares deconvolution of apparent resistivity pseudosections. Geophysics 60 (6), 1682–1690.

Lydersen, E., Larssen, T., Fjeld, E., 2004. The influence of total organic carbon (TOC) on the relationship between acid neutralizing capacity (ANC) and fish status in Norwegian lakes. Sci. Total Environ. 326, 63–69.

Lyngkilde, J., Christensen, T.H., 1992. Redox zones of a landfill leachate pollution plume (Vejen, Denmark). J. Contam. Hydrol. 10, 273–289.

Maechler, M., et al., 2015. Cluster: Cluster Analysis Basics and Extensions. R Package Version 2.0.3.

McArthur, J., et al., 2001. Arsenic in groundwater: testing pollution mechanisms for sedimentary aquifers in Bangladesh. Water Resour. Res. 37 (1), 109–117.

McArthur, J.M., et al., 2004. Natural organic matter in sedimentary basins and its relation to arsenic in anoxic ground water: the example of West Bengal and its worldwide implications. Appl. Geochem. 19 (8), 1255–1293.

McArthur, J.M., Ravenscroft, P., Sracek, O., 2011. Aquifer arsenic source. Nat. Geosci. 4 (10), 655–656.

Mekong River Commission, 2015. Historical Records. http://ffw.mrcmekong.org/historical_rec.htm, last accessed 20 October 2015.

Miller, J.N., Miller, J.C., 2010. Chapter 5: calibration methods in instrumental analysis: regression and correlation. Statistics and Chemometrics for Analytical Chemistry. Pearson Education.

Mukherjee, A., et al., 2008. Hydrogeochemical comparison and effects of overlapping redox zones on groundwater arsenic near the western (Bhagirathi sub-basin, India) and eastern (Meghna sub-basin, Bangladesh) margins of the Bengal Basin. J. Contam. Hydrol. 99, 31–48.

National Institute of Standards and Technology, 2009. Certificate of Analysis: Standard Reference Material 1643e. https://www-s.nist.gov/srmors/certificates/archive/1643e.pdf, accessed 03 Feb 2016.

National Institute of Standards and Technology, 2016. Certificate of Analysis: Standard Reference Material 1640a. https://www-s.nist.gov/srmors/certificates/1640a.pdf, accessed 31 Oct 2016.

Neumann, R.B., et al., 2009. Hydrology of a groundwater-irrigated rice field in Bangladesh: seasonal and daily mechanisms of infiltration. Water Resour. Res. 45, 14.

Neumann, R.B., et al., 2011. Aquifer arsenic source reply. Nat. Geosci. 4 (656). http://dx.doi.org/10.1038/ngeo1278.

Nickson, R.T., et al., 1998. Arsenic poisoning of Bangladesh groundwater. Nature 395, 338.

O'Day, P.A., et al., 2004. The influence of sulfur and iron on dissolved arsenic concentrations in the shallow subsurface under changing redox conditions. Proc. Natl. Acad. Sci. U. S. A. 101 (38), 13703–13708.

Polizzotto, M.L., et al., 2008. Near-surface wetland sediments as a source of arsenic release to ground water in Asia. Nature 454, 505–508.

Polya, D.A., Charlet, L., 2009. Rising arsenic risk? Nat. Geosci. 2 (6), 383–384.

Polya, D.A., et al., 2003. Coupled HPLC-ICP-MS analysis indicates highly hazardous concentrations of dissolved arsenic species in Cambodian groundwaters. R. Soc. Chem. Spec. Publ. 288, 127–140.

Polya, D.A., et al., 2005. Arsenic hazard in shallow Cambodian groundwaters. Mineral. Mag. 69 (5), 807–823.

Polya, D.A., et al., 2017. Groundwater sampling, arsenic analysis and risk communication: Cambodia case study. In: Bhattacharya, P., Polya, D.A., Jovanovic, D. (Eds.), Best Practice Guide for the Control of Arsenic in Drinking Water. IWA Publishing.

Postma, D., et al., 2007. Arsenic in groundwater of the Red River floodplain, Vietnam: controlling geochemical processes and reactive transport modeling. Geochim. Cosmochim. Acta 71 (21), 5054–5071.

R Core Team, 2015. R: A Language and Environment for Statistical Computing. https://www.r-project.org/, last accessed 20 October 2015.

Ravenscroft, P., Brammer, H., Richards, K., 2009. Arsenic pollution — a global synthesis. Royal Geographical Society with IBG. Wiley-Blackwell, Chichester, p. 588.

Rawlins, B.G., et al., 2009. Estimating particle-size fractions of soil dominated by silicate minerals from geochemistry. Eur. J. Soil Sci. 60, 116–126.

Richards, L.A., et al., 2015. Use of lithium tracers to quantify drilling fluid contamination for groundwater monitoring in southeast Asia. Appl. Geochem. 63, 190–202.

Richards, L.A., et al., 2017. Provenance of recharge sources in arsenic-affected groundwaters in Cambodia using stable isotope-based mixing models. J. Hydrol. (under review).

Rowland, H.A.L., et al., 2007. The control of organic matter on microbially mediated iron reduction and arsenic release in shallow alluvial aquifers, Cambodia. Geobiology 5, 281–292.

Rowland, H.A.L., et al., 2008. Geochemistry of aquifer sediments and arsenic-rich groundwaters from Kandal Province, Cambodia. Appl. Geochem. 23 (11), 3029–3046.

Rowland, H.A.L., et al., 2009. The role of indigenous mircoorganisms in the biodegradation of naturally occurring petroleum, the reduction of iron, and the mobilization of arsenite from West Bengal aquifer sediments. J. Environ. Qual. 38 (4), 1598–1607.

Sharif, M.U., et al., 2008. Distribution and variability of redox zones controlling spatial variability of arsenic in the Mississippi River Valley alluvial aquifer, southeastern Arkansas. J. Contam. Hydrol. 99, 49–67.

Smedley, P.L., Edmunds, W.M., 2002. Redox patterns and trace-element behaviour in the East Midlands Triassic Sandstone Aquifer, U.K. Groundwater 40, 44–58.

Smedley, P.L., Kinniburgh, D.G., 2002. A review of the source, behaviour and distribution of arsenic in natural waters. Appl. Geochem. 17 (5), 517–568.

Sovann, C., Polya, D.A., 2014. Improved groundwater geogenic arsenic hazard map for Cambodia. Environ. Chem. 11 (5), 595–607.

Tamura, T., et al., 2007. Depositional facies and radiocarbon ages of a drill core from the Mekong River lowland near Phnom Penh, Cambodia: evidence for tidal sedimentation at the time of Holocene maximum flooding. Asian Earth Sciences]–>J. Asian Earth Sci. 29 (5–6), 585–592.

Tipping, E., Woof, C., Hurley, M.A., 1991. Humic substances in acid surface waters; modelling aluminium binding, contribution to ionic charge-balance, and control of pH. Water Res. 25 (4), 425–435.

Tufano, K.J., et al., 2008. Reductive processes controlling arsenic retention: revealing the relative importance of iron and arsenic reduction. Environ. Sci. Technol. 42, 8283–8289.

USGS, 2015. PHREEQC (Version 3) — A Computer Program for Speciation, Batch-Reaction, One-Dimensional Transport, and Inverse Geochemical Calculations. http://wwwbrr.cr.usgs.gov/projects/GWC_coupled/phreeqc/, last accessed 20 October 2015. (cited 2015; Available from: http://wwwbrr.cr.usgs.gov/projects/GWC_coupled/phreeqc/).

Vandenberghe, J., et al., 1997. New absolute time scale for the Quaternary climate in the Chinese loess region by grain-size analysis. Geology 25 (1), 35–38.

Watts, M.J., et al., 2010. Field based speciation of arsenic in UK and Argentinean water samples. Environ. Geochem. Health 32, 479–490.

World Health Organization, 2011. In: World Health Organization (Ed.), Guidelines for Drinking-water Quality, fourth ed. (Geneva).

Ying, S.C., et al., 2015. Indigenous arsenic (V)-reducing microbial communities in redox-fluctuating near-surface sediments of the Mekong Delta. Geobiology 13 (6), 581–587.